Applied Physics A (2022) 128:944
https://doi.org/10.1007/s00339-022-06087-7

Applied Physics A
Materials Science & Processing

Temporal evolution of optical absorption and emission spectra of thiol capped CdTe quantum dots

Stuti Tomar[1,2] · Suhaas Gupta[3] · Amiya Priyam[4] · Bhavya Bhushan[5] · Arun Singh[6] · Umesh Kumar Dwivedi[7] · Ravi Kant Choubey[1]

Received: 23 July 2022 / Accepted: 23 September 2022

Abstract

To understand the effect of end-groups of thiol-molecules on the structural, absorption, and photoluminescence (PL) properties, CdTe quantum dots (QDs) were synthesized with the capping of thioglycolic acid (TGA), mercaptoethylamine (MEA), L-cysteine (L-Cys) and glutathione (GSH) in aqueous medium. The growth kinetics of the nanocrystals with the variation in the end-groups of thiols has also been spectroscopically investigated. The average sizes of the nanocrystals ranged from 2 to 5 nm, which is well within the quantum confinement regime. The size and phase purity of the QDs were determined by XRD and HRTEM. With respect to size-distribution, the temporal evolution of QDs was found to involve three stages, namely focusing, defocusing and equilibrium. Hydrodynamic sizes were also measured using DLS system. FTIR spectra revealed that the thiol end of the capping agent binds to the particle–surface while the carboxyl or amine group remain free. The multi-colour photoluminescence illustrated the excellent size-tunable optical properties of the QDs. Zeta-potential for TGA-capped CdTe QDs was measured to be −45 mV, indicating high surface charge and hence greater colloidal stability. Such QDs are well suited for bioimaging and therapeutic applications.

Keywords CdTe · Thiol capping · FTIR · Optical absorption · Photoluminescence

1 Introduction

Quantum dots are widely and extensively researched because of their novel properties that are reliably tuneable by varying the size of the nanoparticle [1–3]. Quantum dots are popularly used in optoelectronic devices [4–6], and those optoelectronic properties have been employed in biomedical fields for imaging and sensing applications [7–9], alongside novel applications like drug delivery and therapy [10, 11]. CdTe is a II–VI semiconductor compound which can exhibit luminescence through the entire visible spectrum, which is important for optical applications in biosystems. To make CdTe QDs water-soluble and compatible with biosystems, thiol capped CdTe QDs have been prepared by aqueous synthesis [12, 13], which also increased luminescent stability. These have been used in novel biomedical applications [14] due to the easily tuneable surface properties as a result of different free functional groups of different thiols [15–17].

Murray et al. [12] and Talapin et al. [16] demonstrated the size tunable properties of CdTe QDs, presenting narrow emission peaks over the entire visible spectrum with variation in particle sizes. Talapin et al. [13] observed that

✉ Amiya Priyam
apriyam@cub.ac.in

✉ Ravi Kant Choubey
ravikantchoubey@gmail.com; rkchoubey@amity.edu

[1] Department of Applied Physics, Amity Institute of Applied Sciences (AIAS), Amity University, Noida Campus, Sector-125, Noida, Uttar Pradesh 201313, India

[2] Applied Science and Humanities Department, ABES Engineering College, Campus-1, 19th KM Stone, NH-24, Ghaziabad, Uttar Pradesh 201009, India

[3] Department of Condensed Matter Physics, Faculty of Mathematics and Physics, Charles University, Ke Karlovu 5, 12116 Prague, Czech Republic

[4] Department of Chemistry, School of Physical and Chemical Sciences, Central University of South Bihar, SH-7, Gaya-Panchanpur Road, Gaya 824236, India

[5] Department of Physics, School of Applied Sciences, KIIT, Deemed to be University, Bhubaneswar 751024, India

[6] Department of Physics, Faculty of Natural Sciences, Jamia Millia Islamia Central University, New Delhi 110025, India

[7] Department of Applied Physics, Amity Institute of Applied Sciences, Amity University, Jaipur, Rajasthan, India

Published online: 01 October 2022

capping the CdTe QDs with TOP improved the reaction yield, but reduced the quantum yield of the samples; on the other hand, Wuister et al. [17] observed increased quantum efficiency of CdTe QDs when capped with inorganics. Yu et al. investigated the effects of different capping ligands on the structure and growth of CdTe QDs; Kim et al. synthesised CdTe@CdSe QDs exhibiting increasing red-shift in emission peak with increasing core and shell radii, and Tsay et al. synthesised CdTe@ZnS QDs exhibiting high-intensity narrow emission; Gaponik et al. demonstrated the useful near-IR emission of CdTe QDs; Boldt et al. investigated CdTe QDs in different in different buffers for biolabeling applications, and Zhang et al. investigated the time-dependent emission properties of CdTe QDs in different environments; Gaponik et al. and Zebli et al. separately investigated the labelling of capsules with luminescent CdTe QDs and magnetic nanoparticles for improved targeting and tracing of pathways; these results are summarised in the review articles [1, 7, 9, 11, 14].

Despite the large amount of published research on CdTe QDs and their nanocomposites, there are hardly any report that rigorously investigates the variation of end-groups of thiol capping agents with respect to the optical absorption and photoluminescence of CdTe QDs. These end-groups, such as -COOH in thioglycolic acid (TGA) and $–NH_2$ in mercaptoethylamine (MEA) likely moderate the growth process of QDs to different extent which is not yet fully understood. It is also not known how the simultaneous presence of two end-groups, $–NH_2$ and –COOH as happens in L-cysteine (L-Cys) or Glutathione (GSH) would affect the nucleation and growth kinetics which in turn could affect the surface of QDs and its photoluminescence properties. To design an efficient bioimaging probe, it is imperative that the temporal evolution of the PL properties with these capping agents at different reflux time is thoroughly investigated. To that effect, in the present work, we have synthesised biocompatible and water-soluble CdTe QDs using the different thiols, TGA, MEA, L-Cys and GSH and investigated the optical response of the same as a function of the increasing reflux time. We have analysed the FTIR spectra of the samples to obtain the change in bonds as a result of thiol capping. We have analysed the optical absorption spectra at varying intervals of reflux time to observe the variation in absorption peak, energy band gap, particle size and distribution, and concentration with increasing reflux time; to illustrate the usefulness of the synthesised thiol capped CdTe QDs for biological imaging applications, we have studied variation in the photoluminescent emission spectra with increasing reflux time. Zetapotential investigation was used to obtain the surface charge of the synthesised CdTe QDs as a result of the different thiols used for capping; DLS investigation was used to obtain the hydrodynamic diameter of the synthesised thiol capped CdTe QDs. The authors of the present work plan to use the results of the study as a foundation for future antimicrobial activity testing or investigation into other novel biological applications of the synthesised thiol capped CdTe QDs.

2 Experimental

2.1 Preparation of NaHTe solution

Analytical grade Telluric acid [H_6TeO_6] was obtained from MERCK and used as obtained. A measured amount was dissolved in a minimum amount of deionized water, and the solution was heated with sodium borohydride and continuous flow of nitrogen (N_2) gas. The colour of the solution changed from black (Te) to purple (Te_2^{2-}) to colourless (Te^{2-}). The colourless solution was wrapped tightly with paraffin and cooled overnight. Once the white sodium tetraborate has precipitated, the obtained supernatant liquid is the desired NaHTe.

2.2 Synthesis of thiol capped CdTe quantum dots

Cadmium nitrate tetrahydrate [$Cd(NO_3)_2{\cdot}4H_2O$], Thioglycolic acid [TGA, $C_2H_4O_2S$], Cysteamine [MEA, C_2H_7NS], L-cysteine [L-Cys, $C_3H_7NO_2S$], and Glutathione [GSH, $C_{10}H_{17}N_3O_6S$] were obtained from Sigma-Aldrich at the highest purity available and were used as obtained. Solutions of measured amounts of Cd^{2+} source and thiol were made; pH was maintained between 11.2 and 11.8 for TGA, L-Cys and GSH, and between 5.6 and 6.0 for MEA. The solution was placed in a three-necked flask and deaerated using N_2 gas bubbling for 30 min. During the flow of N_2 and simultaneous stirring, appropriate amount of prepared supernatant NaHTe was injected into the solution, until the final molar ratio of Cd^{2+}:thiol:Te^{2-} in the solution was 1:2.5:0.5. The solution was then refluxed for different total times; 9.5 h for TGA capped CdTe quantum dots (CdTe@TGA QDs), 7.5 h for MEA capped CdTe quantum dots (CdTe@MEA QDs), 4.5 h for L-Cys capped CdTe (CdTe@L-Cys QDs), 2.5 h for GSH capped CdTe (CdTe@GSH QDs). At different time intervals, 1 mL of aliquot was taken from the solutions and used for optical characterisations.

2.3 Characterisations

X-ray diffraction (XRD) was performed on Rigaku Ultima IV X-Ray Diffractometer (Cu Kα radiation, 1.54056 Å) operated at 40 kV and 40 mA with a scanning rate of 0.02°/s. High Resolution Transmission Electron Microscopy (HRTEM) was performed on JEOL JEM-2100F with an accelerating voltage of 200 kV, which also gave us the selected area electron diffraction (SAED) pattern.

Fourier-transform infrared (FTIR) spectroscopy was performed on Shimadzu IRPrestige-21 spectrometer. UV–visible absorption spectroscopy was performed on PerkinElmer LAMBDA 750 in the range 400–700 nm. Photoluminescent emission spectroscopy was performed on Shimadzu RF-5301 PC Spectro fluorophotometer in the range 450–750 nm with an excitation wavelength of 390 nm. Malvern Panalytical Zetasizer Nano ZS was used to perform zetapotential and dynamic light scattering (DLS) measurements.

3 Results and discussion

3.1 XRD analysis

Figure 1 shows the XRD plot of the synthesised TGA-capped CdTe QDs refluxed for 15 min. The characteristic peaks observed are (111), (220) and (311), which matches the bulk cubic CdTe PDF No. 75-2086, confirming the required phase of the synthesised seed cubic CdTe material. PDF No. 75-2086 exhibits the cubic CdTe characteristic high-intensity Bragg diffraction peaks of (111), (220) and (311) at 2θ values of 24.027°, 39.741° and 46.977°, respectively. In comparison, the peak intensities of the same Bragg diffractions in the XRD result of our synthesised CdTe@TGA QDs occurred at slightly higher 2θ values of 24.367°, 40.879° and 47.82°, and exhibit large broadening as a result of small size of crystallite grains, among instrumental and strain broadening effects. Highest intensity (111) peak was analysed to obtain various structural parameters of the synthesised CdTe QDs. We have calculated the lower limit of

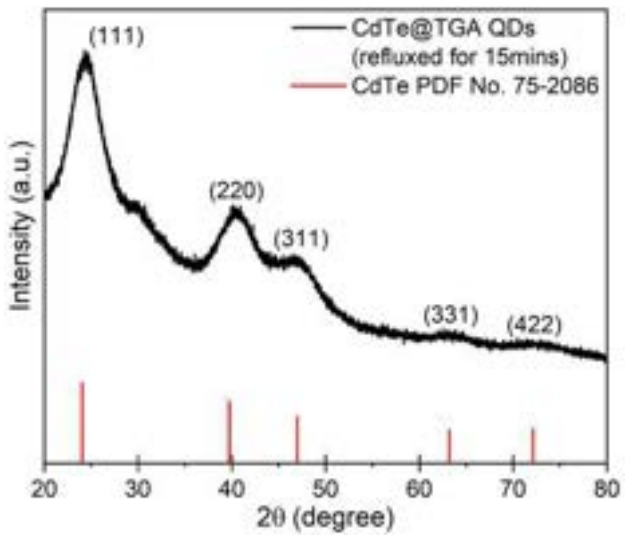

Fig. 1 XRD plot of the synthesised CdTe@TGA QDs refluxed for 15 min

average crystallite size (D) by applying the Scherrer formula, given as follows:

$$D = \frac{k\lambda}{\beta \times \cos\theta},$$

where, k is the sphericity factor, taken as 0.9 for nearly spherical particles, λ is the wavelength of the incoming X-ray radiation (=0.154056 nm for Cu Kα radiation), and β is the FWHM of the characteristic peak centered at Bragg angle 2θ. The lower limit of the crystallite size is calculated as 2.4 nm, which can correspond to a particle diameter ($2r$) of about 3.2 nm from the relation $2r = \frac{4}{3}D$. Interplanar spacing (d_{hkl}) and lattice constant (a) were calculated using the relations,

$$d_{hkl} = \frac{\lambda}{2\sin\theta}$$

$$a = d_{hkl} \times \sqrt{h^2 + k^2 + l^2}$$

For the characteristic (111) peak of our synthesised CdTe@TGA QDs, the calculations yielded interplanar spacing $d_{111} = 3.65$ Å and lattice constant $a_{111} = 6.32$ Å, which is slightly smaller than the lattice constant of 6.41 Å in the cubic CdTe PDF No. 75-2086. The contraction of lattice constant and slight shift of Bragg diffraction peaks with respect to the bulk cubic CdTe PDF No. 75-2086 can be understood as a result of the strong size confinement of our synthesised CdTe@TGA QDs. Broadening of peaks and variation of lattice constant can also occur due to strain on the lattice. Microstructural parameters of microstrain (ε) and dislocation density (δ) were calculated using the following relations:

$$\varepsilon = \frac{\beta}{4\tan\theta}$$

$$\delta = \frac{1}{D^2}$$

For the characteristic (111) peak of our synthesised CdTe@TGA QDs, the calculations yielded micro strain $\varepsilon = 0.069$ and dislocation density $\delta = 17.721 \times 10^{16}$ lines/m^2

3.2 HRTEM and SAED

Figure 2a shows the HRTEM micrograph of the synthesised CdTe@TGA QDs refluxed for 15 min. Average size of the CdTe@TGA QDs as obtained from the micrograph was 3 nm. This is in close agreement with the particle size obtained in the previous section, where the lower limit of average crystallite size calculated using the Scherrer equation underestimates the particle size due to instrumental and strain broadening. Inset in Fig. 2a shows the clearly

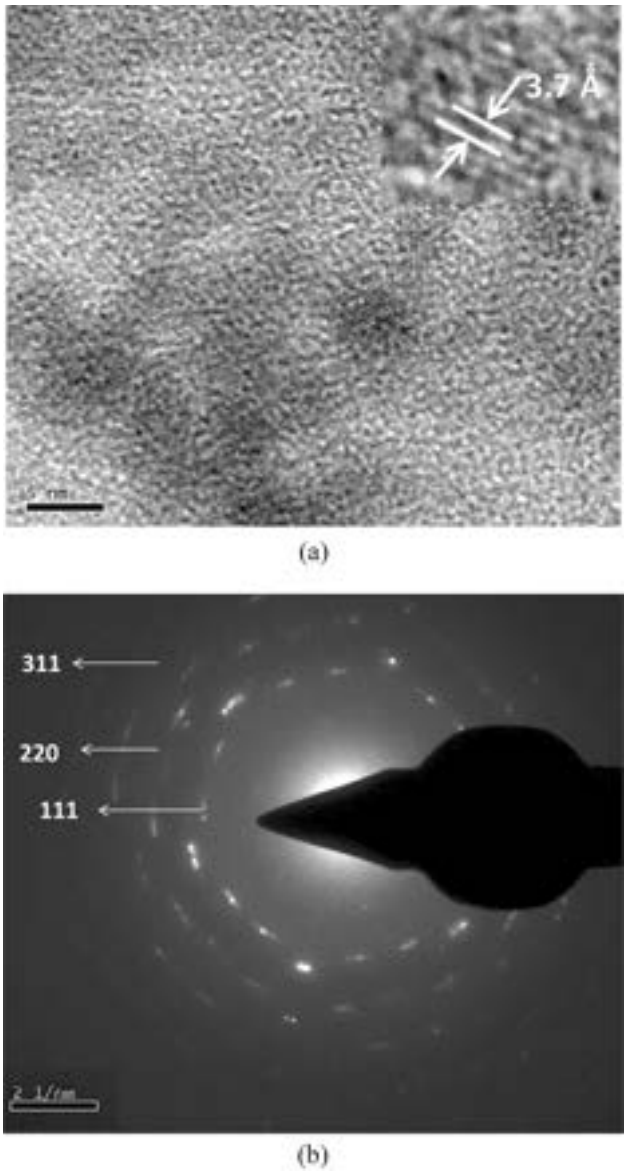

Fig. 2 **a** HRTEM micrograph and **b** SAED pattern of the synthesised CdTe@TGA QDs refluxed for 15 min

discernible lattice fringes, indicating the good crystallinity of the CdTe@TGA QDs, with an interplanar spacing of ~ 3.7 Å, also in close agreement with the interplanar spacing obtained in the previous section. Figure 2b shows the SAED pattern of the synthesised CdTe@TGA QDs refluxed for 15 min. Bright rings corresponding to the reflection from the (111), (220) and (311) planes of the cubic CdTe phase can be clearly observed.

3.3 FTIR spectroscopy

Figure 3a–d shows the FTIR spectra of the synthesised CdTe@TGA, CdTe@MEA, CdTe@L-Cys and CdTe@GSH QDs compared to the FTIR spectra of the thiol used for capping, respectively.

In Fig. 3a, FTIR spectra of TGA exhibits -SH stretching vibration at 2603 cm^{-1}, which is absent in the FTIR spectra of the CdTe@TGA QDs. This is understood as being caused by the cleavage of the thiol H-SR bond and simultaneous formation of the Cd-SR bond. At about 1585 cm^{-1} and 1396 cm^{-1} are peaks corresponding to the asymmetric and symmetric stretching vibrations of $–COO^–$, present in high intensity for the FTIR spectra of both TGA and CdTe@TGA QDs, which indicates that the TGA end group $–COO^–$ remains free in the CdTe@TGA QDs. Peaks at about 2910 cm^{-1} correspond to the symmetric stretching of CH_2, and the peaks at about 1221 cm^{-1} correspond to the wagging vibration of CH_2 [18].

In Fig. 3b, FTIR spectra of MEA exhibits -SH stretching vibration at 2493 cm^{-1}, which is absent in the FTIR spectra of the CdTe@MEA QDs, attributed to the cleavage of the H-SR bond and simultaneous formation of the Cd-SR bond. High intensity peak at about 1581 cm^{-1} corresponds to N–H vibrations, present in the FTIR spectra of both MEA and CdTe@MEA QDs, indicating that the MEA end group N–H remains free in the CdTe@MEA QDs. Peaks between 1400 and 1000 cm^{-1} are attributed to different CH_2 vibrations [19, 20].

In Fig. 3c, FTIR spectra of L-Cys exhibits –SH stretching vibration at 2563 cm^{-1}, whose absence in the FTIR spectra of the CdTe@L-Cys QDs is attributed to the cleavage of the H-SR bond and simultaneous formation of the Cd-SR bond. Peaks at about 1579 cm^{-1} and 1392 cm^{-1} correspond to the asymmetric and symmetric stretching vibrations of $–COO^–$, and its presence in the FTIR spectra of both L-Cys and CdTe@L-Cys QDs indicates the L-Cys end group $–COO^–$ remains free in the CdTe@L-Cys QDs. Peaks between 1350 and 1000 cm^{-1} are attributed to different CH_2 vibrations [21–23].

In Fig. 3d, FTIR spectra of GSH exhibits –SH stretching vibration at 2603 cm^{-1}, whose absence in the FTIR spectra of the CdTe@GSH QDs is attributed to the cleavage of the H–SR bond and simultaneous formation of the Cd–SR bond. Peak at about 1595 cm^{-1} corresponds to the N–H vibration and its presence in the FTIR spectra of both GSH and CdTe@GSH indicates the GSH amide end group remains free in the CdTe@GSH QDs. Peaks at about 1390 cm^{-1} and 1042 cm^{-1} correspond to the C–S and C–N stretching, respectively [24, 25].

3.4 UV–visible absorption spectroscopy

Figure 4a–d shows the UV–visible absorption spectra of the synthesised CdTe@TGA, CdTe@MEA, CdTe@L-Cys QDs and CdTe@GSH QDs, respectively, at different times of reflux. All QDs exhibit blue shift of the absorption peak

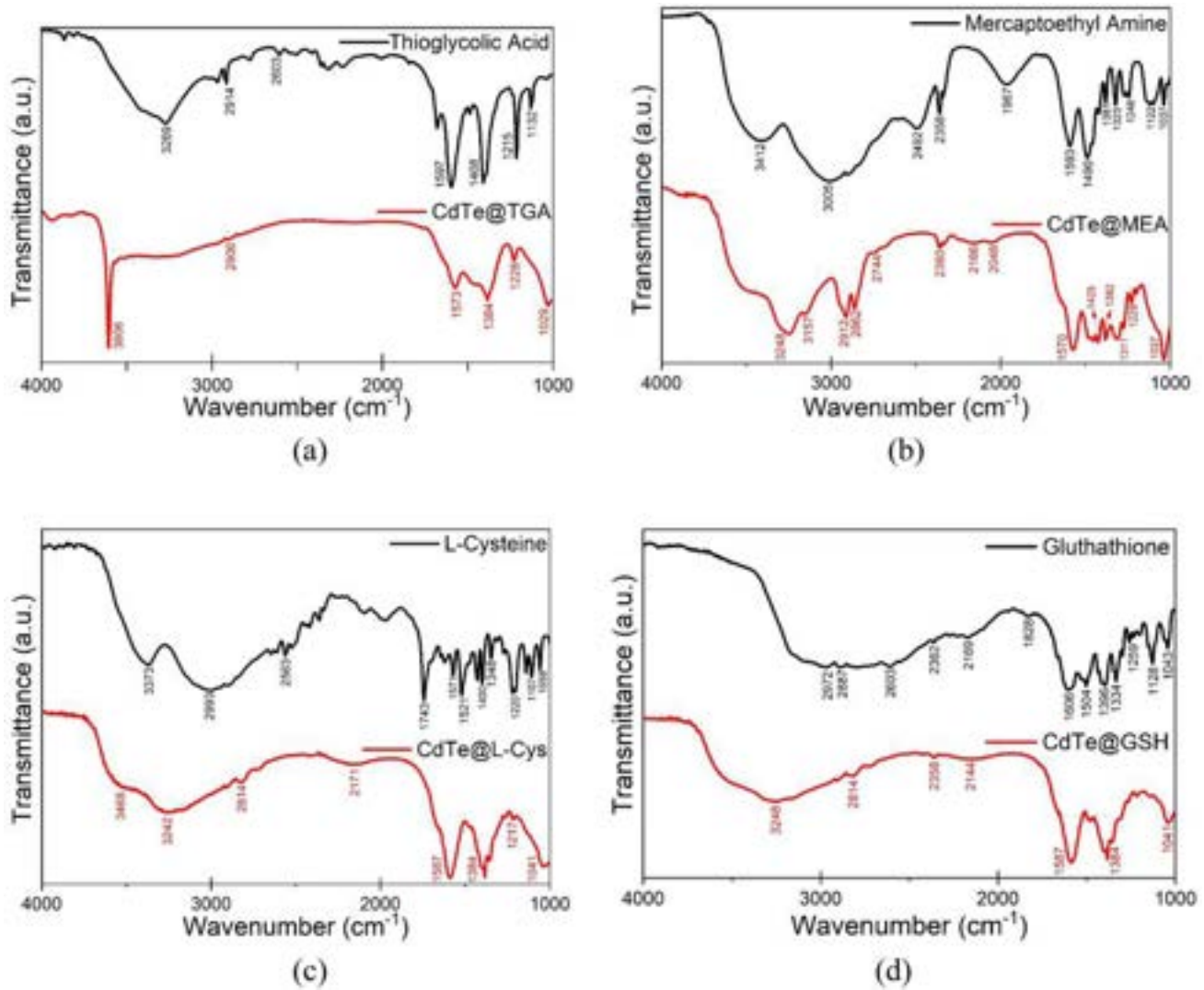

Fig. 3 FTIR spectra of **a** thioglycolic acid (TGA) and CdTe@TGA QDs, **b** mercaptoethyl amine (MEA) and CdTe@MEA QDs, **c** L-Cysteine (L-Cys) and CdTe@L-Cys QDs, and **d** glutathione (GSH) and CdTe@GSH

with respect to bulk CdTe (~800 nm), indicating strong size confinement of the thiol-capped CdTe QDs. As reflux time is increased, a corresponding gradual shift in the absorption peak to longer wavelengths is observed for all QDs, indicating a trend of increasing particle size with reflux time. 1st derivative of the UV–visible absorption v/s energy plot was fitted with a Gaussian peak, and the peak position obtained is the energy band gap of the QD sample (E_g^{nano}). Table 1 shows the variation in obtained E_g^{nano} of the synthesised thiol capped CdTe QDs with different reflux times. Absorption edge (λ_a) was calculated from E_g^{nano} using the following equation:

$$\lambda_a = \frac{hc}{E_g^{nano}},$$

where h and c are the Planck's constant and the speed of light in vacuum, respectively. Table 2 shows the variation in calculated λ_a of the synthesised thiol capped CdTe QDs with different reflux times. E_g^{nano} larger than the energy band gap of bulk CdTe ($E_g^{bulk} = 1.44$ eV) confirms the strong size confinement of the thiol capped CdTe QDs. Tight binding approximation model was used to calculate the size of the nanoparticle (d) using the following equation:

$$\Delta E_g = a_1 \times e^{-d/b_1} + a_2 \times e^{-d/b_2},$$

where $\Delta E_g = E_g^{nano} - E_g^{bulk}$; $a_1 = 5.77$, $a_2 = 1.33$, $b_1 = 8.45$ and $b_2 = 43.73$ for CdTe [26, 27]. Table 3 shows the variation in calculated particle size with reflux time for the thiol capped CdTe QDs. General trend of increasing particle size with increasing reflux time suggests the growth of the

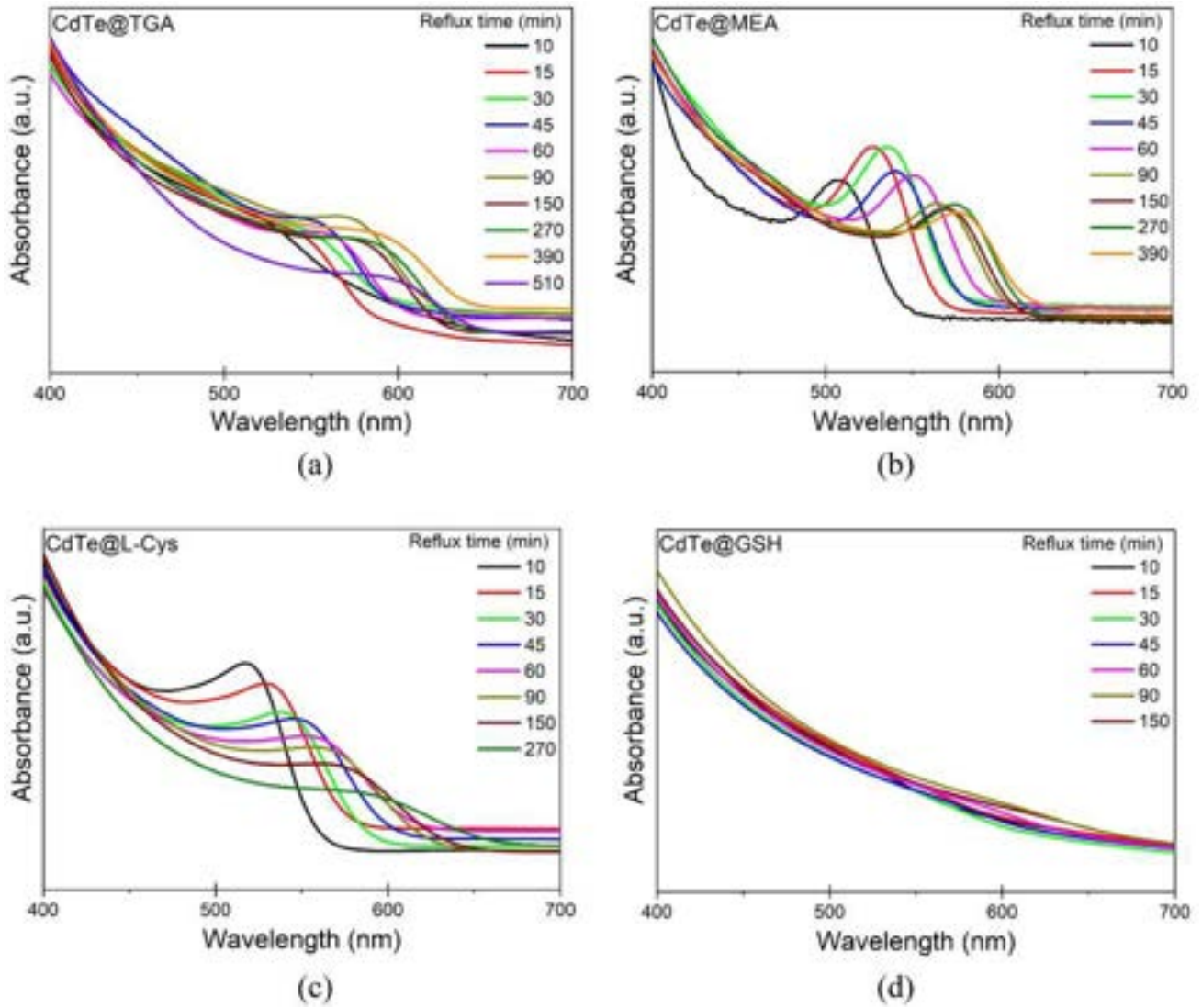

Fig. 4 UV–visible absorption spectra of **a** CdTe@TGA QDs, **b** CdTe@MEA QDs, **c** CdTe@L-Cys QDs, and **d** CdTe@GSH QDs at different reflux times

Table 1 Variation in the energy band gap obtained from the peak of the 1st derivative of UV–visible absorption v/s energy plot of the synthesised thiol capped CdTe QDs with different reflux times

ENERGY BAND GAP (E_g^{nano}, eV)	Reflux time (minutes)									
QD sample	10	15	30	45	60	90	150	270	390	510
CdTe@TGA	2.26	2.17	2.17	2.15	2.12	2.07	2.05	2.02	2	1.99
CdTe@MEA	2.34	2.25	2.22	2.2	2.16	2.1	2.09	2.07	2.06	–
CdTe@L-Cys	2.28	2.23	2.18	2.14	2.10	2.07	2.04	1.98	–	–
CdTe@GSH	2.29	2.21	2.17	2.13	2.05	1.98	1.94	–	–	–

nanoparticles are governed by Ostwald ripening. Larger particles exhibit energetically favourable stability as compared to smaller particles, therefore, as the solution is heated, slow diffusion of materials from smaller nanoparticles to the surface of the larger nanoparticles takes place, thus increasing the particle size continuously during growth [28].

Figure 5 shows the variation in calculated particle size with reflux time for the thiol-capped CdTe QDs.

Table 2 Variation in the absorption peak calculated from the energy band gap of the synthesised thiol capped CdTe QDs with different reflux times

ABSORPTION PEAK (λ_a, nm)	Reflux time (minutes)									
QD sample	10	15	30	45	60	90	150	270	390	510
CdTe@TGA	548	571	571	576	584	599	604	613	620	623
CdTe@MEA	529	551	558	563	574	590	593	599	601	–
CdTe@L-Cys	543	556	568	579	590	599	607	626	–	–
CdTe@GSH	541	561	571	582	604	626	639	–	–	–

Table 3 Variation in particle size calculated from the energy band gap of the synthesised thiol capped CdTe QDs with different reflux times

Particle size (d, nm)	Reflux time (minutes)									
QD sample	10	15	30	45	60	90	150	270	390	510
CdTe@TGA	3	3.3	3.3	3.4	3.5	3.7	3.8	4	4.1	4.1
CdTe@MEA	2.8	3	3.1	3.2	3.3	3.5	3.6	3.7	3.8	–
CdTe@L-Cys	2.9	3.1	3.3	3.4	3.5	3.7	3.9	4.2	–	–
CdTe@GSH	2.9	3.2	3.3	3.5	3.8	4.2	4.3	–	–	–

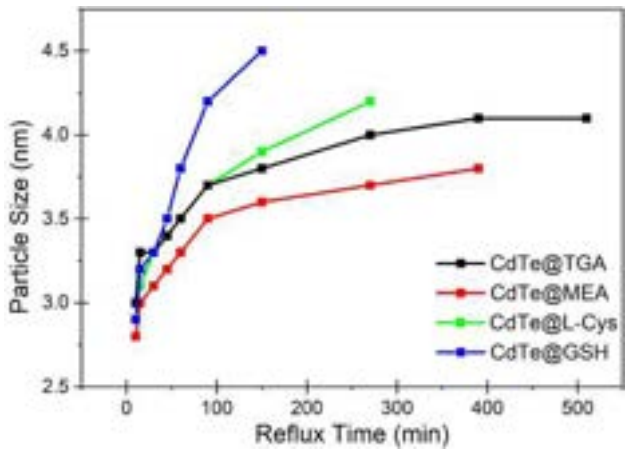

Fig. 5 Particle size v/s reflux time of the thiol-capped CdTe QDs

Synthesis time required to attain a predetermined particle size increases considerably upon replacing TGA with MEA in the synthesis process; to attain a particle size of 3.7 nm, the solution containing CdTe@TGA QDs was refluxed for 90 min, while the solution containing CdTe@MEA QDs was refluxed for 270 min. When both end groups are simultaneously present, like in the CdTe@L-Cys QDs, the reflux time to attain a particle size greater than 4 nm is considerably smaller than the reflux time required for both CdTe@TGA and CdTe@MEA QDs. Replacing L-Cys with GSH in the synthesis process even more drastically brings down the time to attain a predetermined particle size; the CdTe@GSH QDs attained a particle size of greater than 4 nm in just 90 min and a particle size of 4.5 nm in 150 min. Figure 6a–d shows the variation of the particle size and concentration of the synthesised CdTe@TGA, CdTe@MEA, CdTe@L-Cys QDs and CdTe@GSH QDs, respectively, with increasing reflux time. Correlation between the particle diameter and the extinction coefficient [29] was employed to obtain the concentrations at different reflux times using the absorbance values at λ_a. Primary analysis of the plots reveal that with increasing particle size and reflux time the concentration of quantum dots decays exponentially, suggesting a good separation between the nucleation and growth processes for the thiol-capped CdTe QDs [3, 30], i.e., monomer units generated in the initial supersaturation phase are instantly used for the formation of nucleation centers, and subsequent growth of the larger nanoparticles takes place at the expense of smaller nanoparticles, thereby decreasing the concentration.

Figure 7a–d shows the variation of particle size and $\Delta\lambda$ of the synthesised CdTe@TGA, CdTe@MEA, CdTe@L-Cys and CdTe@GSH QDs, respectively, with increasing reflux time. $\Delta\lambda = \lambda_a - \lambda_{onset}$, i.e., the difference between the onset of absorption and the absorption edge is a measure of the particle size distribution similar to FWHM; larger $\Delta\lambda$ suggests a larger size distribution and vice versa [3, 31, 32]. Three regimes of growth have been identified in all the plots: (i) focussing, (ii) defocussing, and (iii) equilibrium. Initially, smaller agglomerates in the solution grow faster as compared to the larger nanoparticles, leading to a reduction, or focussing of the particle size distribution. As more time passes, Ostwald ripening processes dominate and nanoparticle growth is facilitated by the decrease in size of smaller agglomerates and increase in size of larger agglomerates, leading to the increase in particle size distribution during the defocussing stage. Eventually, the smallest agglomerates dissolve completely into the larger agglomerates, and further nanoparticle growth takes place at an 'equilibrium' size distribution.

Figure 8 shows the variation in growth rate (dr/dt) with $1/r$ (where r is the particle radius) for the thiol-capped

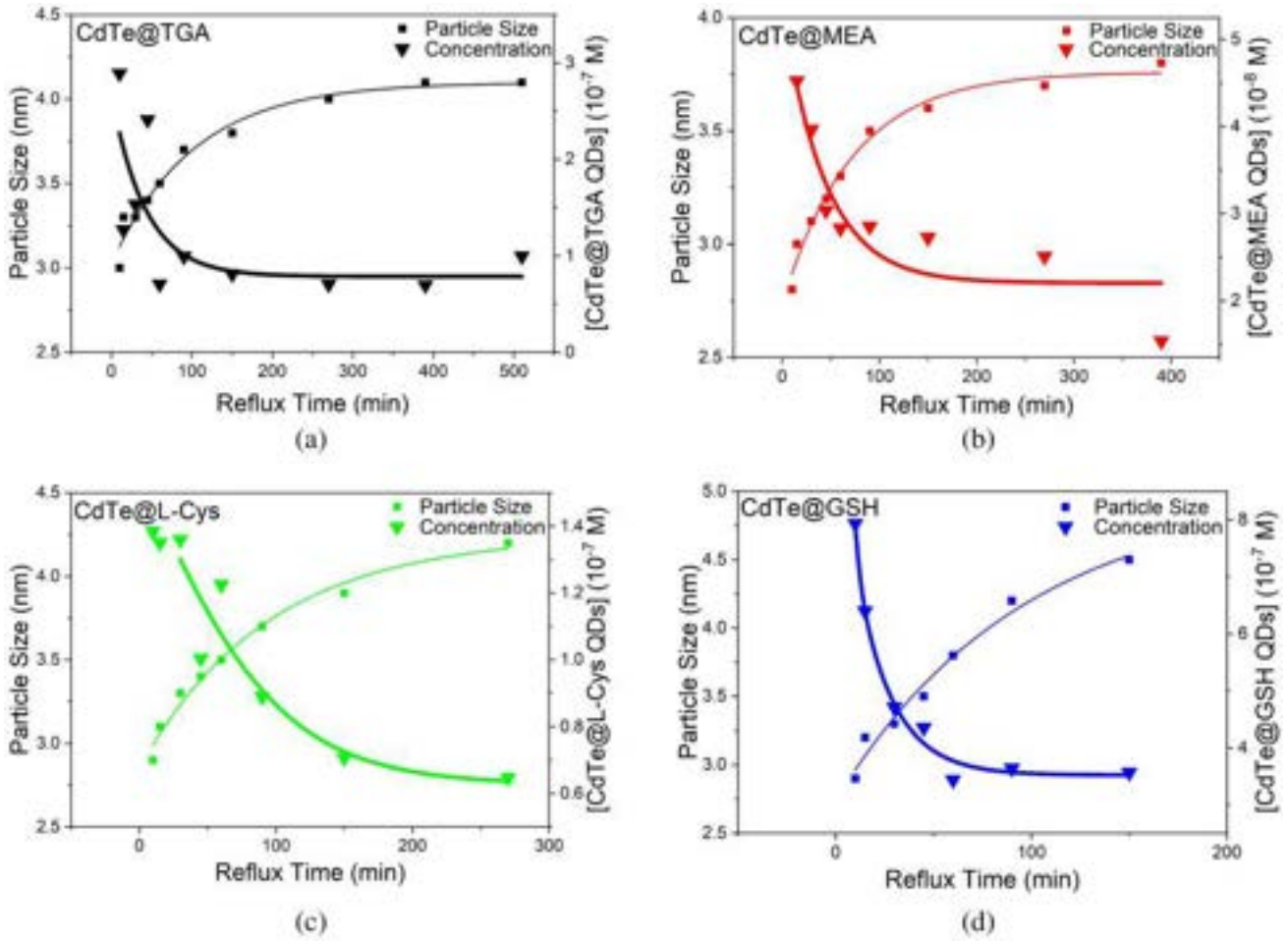

Fig. 6 **a** Particle size and concentration v/s reflux time of the CdTe@TGA QDs. **b** Particle size and concentration v/s reflux time of the CdTe@MEA QDs. **c** Particle size and concentration v/s reflux time of the CdTe@L-Cys QDs. **d** Particle size and concentration v/s reflux time of the CdTe@GSH QDs

CdTe QDs; for all four different thiol-capped CdTe QDs the growth rate showed a steady decline with increasing particle size. Regression analysis revealed a linear relationship between dr/dt and 1/r, which obeys the particle growth rate equation developed by Sugimoto [33] under pure diffusion control condition (later modified by Talapin et al. [34] for particle growth under various control conditions) given as follows:

$$\frac{\mathrm{d}r}{\mathrm{d}t} = DV_{\mathrm{m}}\left(\frac{1}{r} - \frac{1}{\delta}\right)\left\{[M]_{\mathrm{bulk}} - C(r)\right\},$$

where D is the diffusion coefficient of the monomer, V_{m} is the molar volume of the solid, δ is the diffusion layer thickness, and the term $\{[M]_{\mathrm{bulk}} - C(r)\}$ is assumed to be constant for the given conditions, where $[M]_{\mathrm{bulk}}$ is the monomer concentration in the bulk of the solution and $C(r)$ is the solubility of a particle with radius = r. As reported before [35], initial growth rate in the presence of L-Cys is greater than the initial growth rate in the presence of MEA, attributed to the greater surface tension at the nanoparticle–solvent interface for the CdTe QDs synthesised in the presence of L-Cys, as compared to the CdTe QDs synthesised in the presence of MEA. Similarly, CdTe QDs synthesised in the presence of TGA show the highest initial growth rate, attributed to the greatest electrostatic repulsion amongst the negatively charged (ionised carboxyl group) TGA molecules.

3.5 Photoluminescent emission spectroscopy

Figure 9a–d shows the photoluminescence spectra of the synthesised CdTe@TGA, CdTe@MEA, CdTe@L-Cys and CdTe@GSH QDs, respectively, at different times of reflux; all the samples exhibit strong single peak emission with narrow widths, especially at lower reflux times. As reflux time is increased, a corresponding gradual shift in the emission peak to longer wavelengths is observed for all QDs, indicating a trend of increasing particle size with reflux time. Table 4 shows the variation in the emission peak with reflux

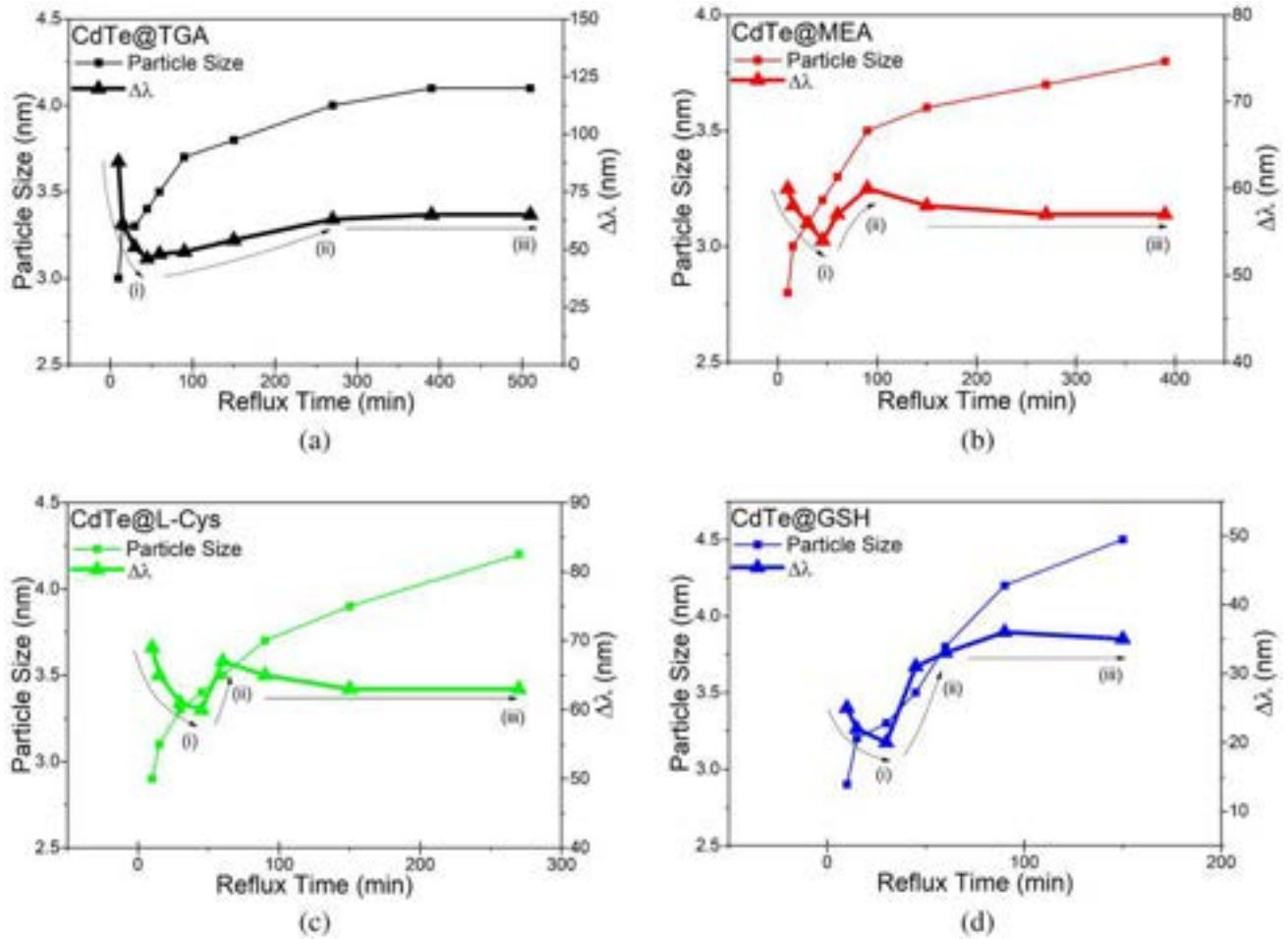

Fig. 7 Particle size and $\Delta\lambda$ v/s reflux time of the **a** CdTe@TGA QDs, **b** CdTe@MEA QDs, **c** CdTe@L-Cys QDs and **d** CdTe@GSH QDs

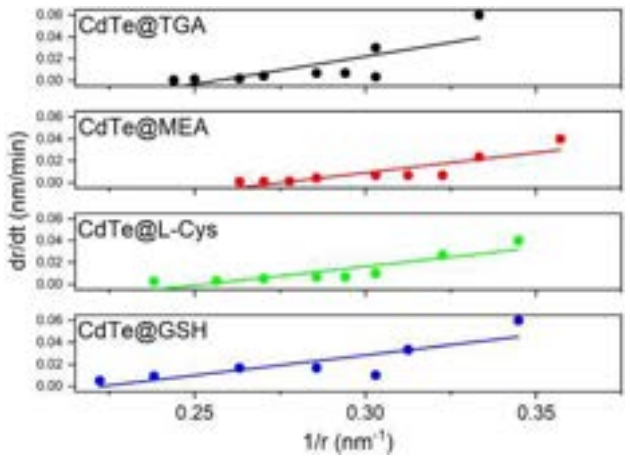

Fig. 8 d*r*/d*t* v/s 1/*r* of the thiol-capped CdTe QDs

time for the thiol capped CdTe QDs. At 10 min of reflux time, the CdTe@TGA, CdTe@L-Cys and CdTe@GSH QDs exhibit green–yellow emission (~ 557 nm); CdTe@TGA QDs are the first to start emitting strongly in the yellow colour region (573 nm) at just 15 min of reflux time. At 10 min of reflux time, CdTe@MEA QDs exhibit a greener emission (536 nm) than the rest of the synthesised samples, and by 150 min of reflux time the CdTe@MEA QDs exhibit a yellow-orange emission (593 nm). At the end of appropriate amount of reflux time, the CdTe@TGA, CdTe@L-Cys and CdTe@GSH QDs are emitting strongly in the red colour region (~ 638 nm).

The full-width at half-maximum (FWHM) of an emission intensity peak qualitatively illustrates the size distribution of the particles in the sample under analysis; larger FWHM suggest a larger size distribution and vice versa. In the PLE spectra of the CdTe@L-Cys QDs refluxed for 150 min and 270 min, it is possible to deconvolute the emission peak into two (or more) Gaussian peaks, as illustrated in the inset of Fig. 9c, to further try to understand the contributions of emission from different sized particles in the sample. At 150 min, the contributions from the two deconvoluted peaks, representing the emission from two different sized particles,

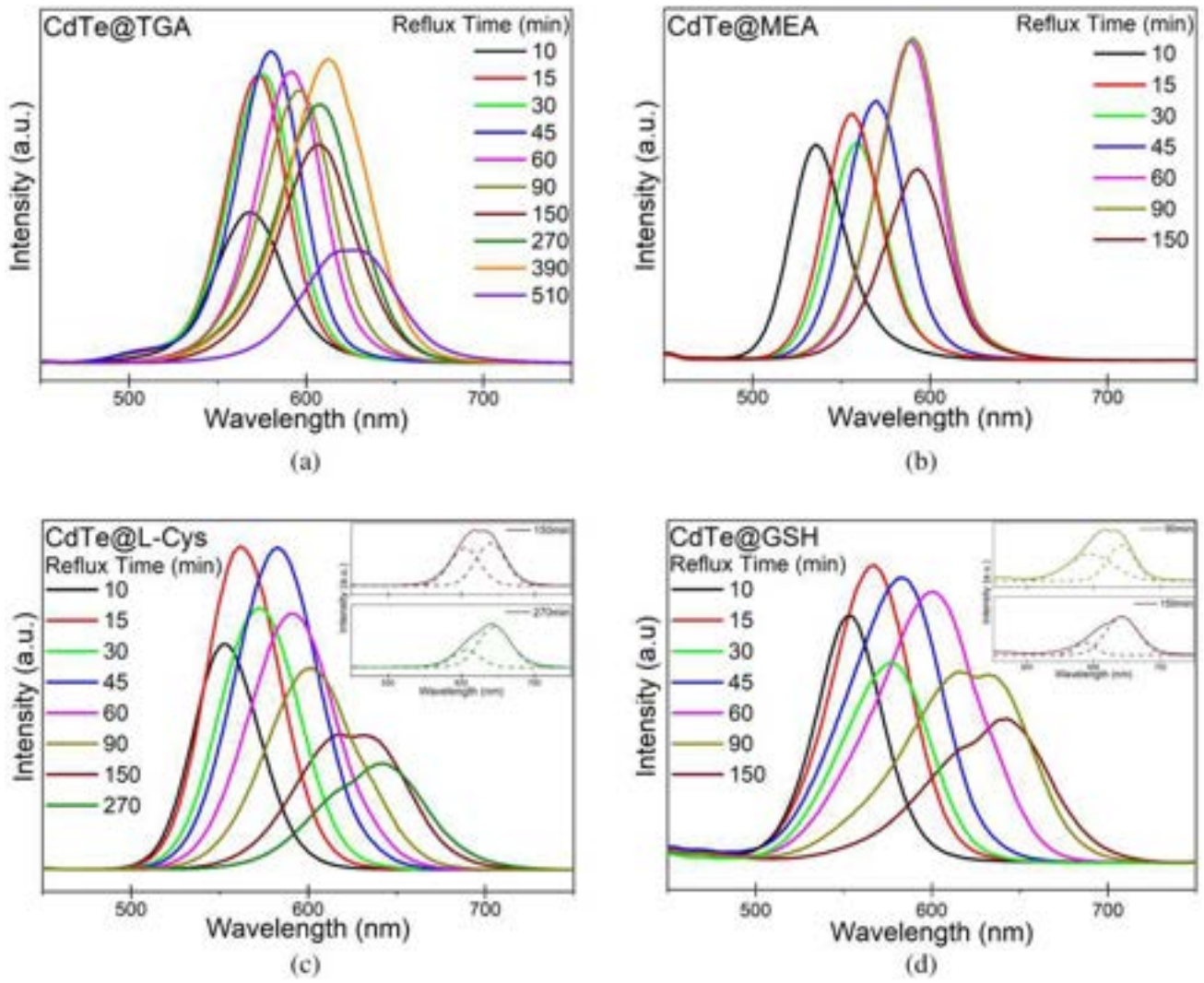

Fig. 9 Photoluminescent emission spectra of **a** CdTe@TGA QDs, **b** CdTe@MEA QDs, **c** CdTe@L-Cys QDs and **d** CdTe@GSH QDs at different reflux times

Table 4 Variation in the emission peak of the synthesised thiol capped CdTe QDs with different reflux times

Emission peak (nm)	Reflux time (minutes)									
QD Sample	10	15	30	45	60	90	150	270	390	510
CdTe@TGA	568	573	575	580	592	596	606	608	612	627
CdTe@MEA	536	556	560	570	588	590	593	–	–	–
CdTe@L-Cys	553	562	572	583	590	602	640[a]	645[a]	–	–
CdTe@GSH	552	567	577	583	601	641[a]	642[a]	–	–	–

[a]Given values are the photoluminescent emissions at longer wavelength of the two peaks deconvoluted from the PLE spectra of the thiol capped QD at that reflux time

to the total PLE of the sample is nearly equal. Comparatively, in the CdTe@L-Cys QD refluxed for 270 min, the contribution of the deconvoluted peak at higher wavelength is larger, i.e., the intensity of emission by the larger sized particles is greater than that of the smaller sized particles, indicating the shift of the particle size distribution to higher sizes with increasing reflux times. Similarly, inset of Fig. 9d shows the deconvolution of the PLE spectra of the CdTe@GSH QDs refluxed for 90 min and 150 min. As before, with increasing reflux time, the emission intensity contribution

of the larger sized particles increases, indicating the shift of particle size distribution to higher sizes with increasing reflux times.

3.6 Zetapotential

A layer of surface charges forms around a particle dispersed in an aqueous medium, and the potential at the boundary of the layer (slipping plane) is called the zetapotential. Among other factors, it plays a role in mediating interparticle interactions [36]. Table 5 shows the zetapotential of the thiol capped CdTe QDs at a pH of 9. CdTe@TGA QDs have a negative surface charge due to the presence of $-COO^-$ group, while CdTe@MEA QDs have a positive surface charge due to the presence of protonated amino group ($-NH_3^+$). CdTe@L-Cys and CdTe@GSH QDs carry a similar negative surface charge of −33 mV and −31 mV, respectively, less than the CdTe@TGA QDs which has the highest absolute zetapotential value of all the samples (−45 mV). Highest absolute zetapotential value of the CdTe@TGA QDs indicate that the TGA capping on the CdTe QDs has greatly increased their colloidal stability in comparison to capping with other thiols; this is evident by the higher initial growth rate of the CdTe@TGA QDs. Capping with L-Cys or GSH lends moderate colloidal stability to the CdTe QDs, while capping with MEA induces a higher tendency of coagulation in the CdTe QDs at pH 9. However, CdTe@MEA QDs exhibit a positive zetapotential (+0.5 mV), which indicates usefulness for applications in biological fields, as most proteins have a positive or neutral surface charge.

Table 5 Zetapotential of the synthesised thiol capped CdTe QDs at a pH of 9

QD sample	Zetapotential (mV) at pH 9
CdTe@TGA	−45
CdTe@MEA	0.5
CdTe@L-Cys	−33
CdTe@GSH	−31

3.7 DLS measurements

DLS measurements help us obtain the hydrodynamic diameter of the sample. Figure 10a and b show the size distribution histograms obtained from DLS measurements for CdTe@TGA and CdTe@L-Cys QDs, respectively, after 15 min of reflux time. The average hydrodynamic diameter for both the samples is around 6.8 nm, with a particle size distribution ranging from 5 to 10 nm. For the same reflux time, particle size calculated by the tight binding approximation was 3.4 nm for both samples. Since the light scattering fluctuations measured in the DLS technique depends also on the surface structure of the surface bound thiols, overall size obtained from the DLS technique is larger than that obtained from calculations done on the UV–visible absorption spectra, which corresponds to the energy band gap of the core CdTe. However, CdTe QDs capped with L-Cys, which is a larger polymer than TGA, exhibit smaller hydrodynamic diameter and wider size distribution than the CdTe@TGA QDs, for the same reflux time. This can be understood as a consequence of the higher initial growth rate of the CdTe@TGA QDs, as observed in the previous section.

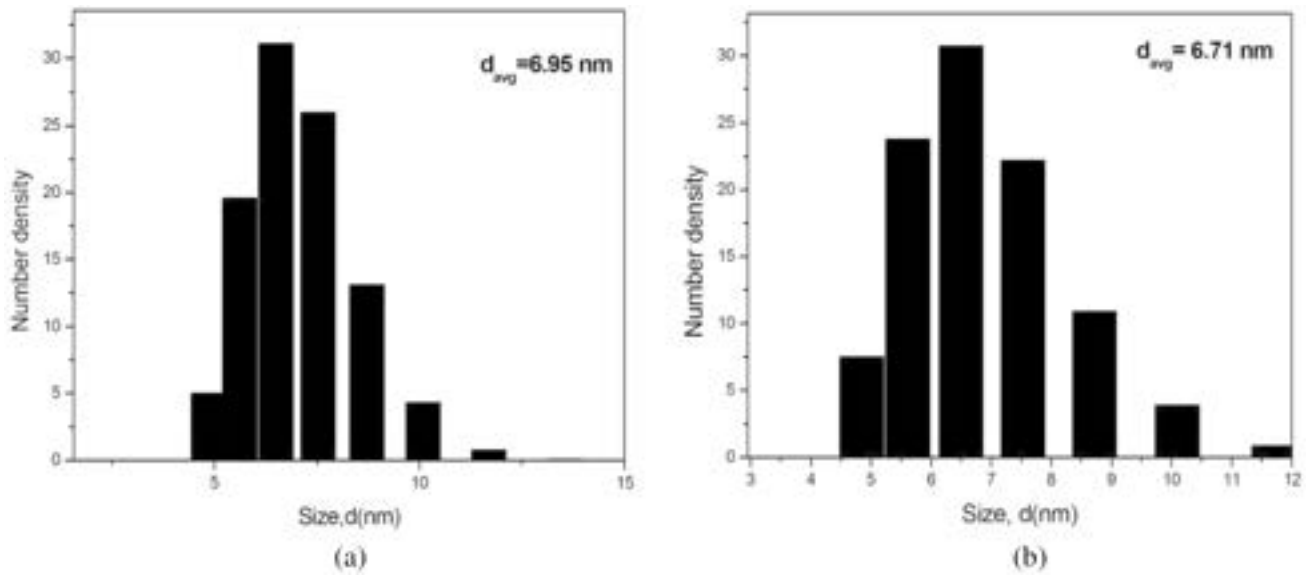

Fig. 10 Size distribution histogram in terms of hydrodynamic diameter for **a** CdTe@TGA QDs and **b** for CdTe@L-Cys QDs refluxed for 15 min

4 Conclusions

In the present work CdTe QDs were synthesised with different thiol capping of TGA, MEA, L-Cys and GSH using prepared NaHTe solution. XRD pattern of the synthesised thiol-capped QDs confirmed the cubic CdTe phase of the synthesized material, further supported by the HRTEM micrograph and SAED pattern. FTIR spectra of the thiols exhibit the -SH stretching vibration peak at an average of 2553 cm^{-1}, which is absent in the FTIR spectra of the synthesised CdTe@TGA, CdTe@MEA, CdTe@L-Cys and CdTe@GSH QDs, attributed to the cleavage of the H-SR bond and simultaneous formation of the Cd-SR bond. UV–visible absorption spectra of the thiol-capped CdTe QDs exhibited blue shift in absorption peak as compared to that of bulk CdTe, indicating strong size confinement in the synthesised QDs. Gradual shift of the absorption peaks towards longer wavelengths is observed with increasing reflux time of all the thiol capped CdTe QDs. Energy band gap values were obtained from the absorption spectra, and used with the Tight Binding approximation to obtain change in particle size with reflux time; growth in the size of particle continued with an increasing reflux time, before reaching a plateau. To attain a predetermined size of nanoparticle, CdTe@GSH QDs took the least reflux time, followed closely by CdTe@L-Cys and then CdTe@TGA QDs, while the reflux time for CdTe@MEA QDs to attain the predetermined nanoparticle size was considerably larger. Concentration was obtained from the correlation between extinction coefficient, particle diameter and absorbance; concentration of the thiol-capped CdTe QDs was found to decay exponentially with increasing reflux time and particle size. Change in particle size distribution with reflux time was obtained using the difference between the onset of absorption and the absorption edge; three distinct regimes (focussing, defocussing and equilibrium) of nanoparticle growth were observed. PLE spectra of the thiol capped CdTe QDs exhibited strong single peak emissions with narrow widths from green to orange range with increasing reflux times. At pH 9, CdTe@TGA QDs exhibited a more negative zetapotential than CdTe@L-Cys and CdTe@GSH QDs, indicating higher colloidal stability, while CdTe@MEA QDs exhibited a small positive zetapotential, useful for biological applications. Hydrodynamic diameter of the CdTe@TGA and CdTe@L-Cys was larger than the particle size obtained from the Tight Binding approximation, which is a result of the optical response of the core QD material.

Author contributions All the authors contributed to the present work, conception and design, Material preparation, data collection and analysis were performed by the authors. The author's contribution is shown below. The first draft of the manuscript was written by Stuti Tomar and Suhaas Gupta and all the authors commented on the previous version of the manuscript. All the authors read and approved the final manuscript.

Research data policy and data availability statements All data generated or analysed during this study have been deposited in this manuscript. All the compared data were properly cited and included in the reference section following the journal style. Also, the data will be available from the corresponding author on reasonable request.

Declarations

Conflict of interest In this manuscript, there is no conflict of interest.

Consent for publication I hereby confirm that, the work described has not been published before; it is not under consideration for publication anywhere else; and publication has been approved by all co-authors of this manuscript.

References

1. Y. Yin, A.P. Alivisatos, Colloidal nanocrystal synthesis and the organic–inorganic interface. Nature **437**(7059), 664–670 (2005)
2. A. Shavel, N. Gaponik, A. Eychmüller, Factors governing the quality of aqueous CdTe nanocrystals: calculations and experiment. J. Phys. Chem. B **110**(39), 19280–19284 (2006)
3. A. Priyam, A. Chatterjee, S.C. Bhattacharya, A. Saha, Surface-functionalized cadmium chalcogenide nanocrystals: a spectroscopic investigation of growth and photoluminescence. J. Cryst. Growth **304**(2), 416–424 (2007)
4. A.M. Kapitonov, A.P. Stupak, S.V. Gaponenko, E.P. Petrov, A.L. Rogach, A. Eychmüller, Luminescence properties of thiol-stabilized CdTe nanocrystals. J. Phys. Chem. B **103**(46), 10109–10113 (1999)
5. S. Gupta, R.K. Choubey, L.K. Sharma, M.P. Ghosh, M. Kar, S. Mukherjee, Exploring the magnetic ground state of vanadium doped zinc sulphide. Semicond. Sci. Technol. **34**(10), 105006 (2019)
6. S. Tomar, S. Gupta, S. Mukherjee, A. Singh, S. Kumar, R.K. Choubey, Manganese-doped ZnS QDs: an investigation into the optimal amount of doping. Semiconductors **54**(11), 1450–1458 (2020)
7. X. Gao, Y. Cui, R.M. Levenson, L.W. Chung, S. Nie, In vivo cancer targeting and imaging with semiconductor quantum dots. Nat. Biotechnol. **22**(8), 969–976 (2004)
8. C.Y. Zhang, H.C. Yeh, M.T. Kuroki, T.H. Wang, Single-quantum-dot-based DNA nanosensor. Nat. Mater. **4**(11), 826–831 (2005)
9. I.L. Medintz, H.T. Uyeda, E.R. Goldman, H. Mattoussi, Quantum dot bioconjugates for imaging, labelling and sensing. Nat. Mater. **4**(6), 435–446 (2005)
10. L. Qi, X. Gao, Emerging application of quantum dots for drug delivery and therapy. Expert Opin. Drug Deliv. **5**(3), 263–267 (2008)
11. A.C. Samia, S. Dayal, C. Burda, Quantum dot-based energy transfer: perspectives and potential for applications in photodynamic therapy. Photochem. Photobiol. **82**(3), 617–625 (2006)
12. C. Murray, D.J. Norris, M.G. Bawendi, Synthesis and characterization of nearly monodisperse CdE (E = sulfur, selenium, tellurium) semiconductor nanocrystallites. J. Am. Chem. Soc. **115**(19), 8706–8715 (1993)
13. D.V. Talapin, S. Haubold, A.L. Rogach, A. Kornowski, M. Haase, H. Weller, A novel organometallic synthesis of highly luminescent CdTe nanocrystals. J. Phys. Chem. B **105**(12), 2260–2263 (2001)

14. N. Gaponik, A.L. Rogach, Thiol-capped CdTe nanocrystals: progress and perspectives of the related research fields. Phys. Chem. Chem. Phys. **12**(31), 8685–8693 (2010)
15. W.W. Yu, X. Peng, Formation of high-quality CdS and other II–VI semiconductor nanocrystals in noncoordinating solvents: tunable reactivity of monomers. Angew. Chem. Int. Ed. **41**(13), 2368–2371 (2002)
16. D.V. Talapin, A.L. Rogach, I. Mekis, S. Haubold, A. Kornowski, M. Haase, H. Weller, Synthesis and surface modification of amino-stabilized CdSe, CdTe and InP nanocrystals. Colloids Surf., A **202**(2–3), 145–154 (2002)
17. S.F. Wuister, C. de Mello Donega, A. Meijerink, Influence of thiol capping on the exciton luminescence and decay kinetics of CdTe and CdSe quantum dots. J. Phys. Chem. B **108**(45), 17393–17397 (2004)
18. T. Kondratenko, O. Ovchinnikov, I. Grevtseva, M. Smirnov, O. Erina, V. Khokhlov, B. Darinsky, E. Tatianina, Thioglycolic acid FTIR spectra on Ag2S quantum dots interfaces. Materials **13**(4), 909 (2020)
19. K. Rajar, A. Balouch, M.I. Bhanger, M.T. Shah, T. Shaikh, S. Siddiqui, Succinic acid functionalized silver nanoparticles (Suc-Ag NPs) for colorimetric sensing of melamine. Appl. Surf. Sci. **435**, 1080–1086 (2018)
20. M.T. Yaraki, M. Tayebi, M. Ahmadieh, M. Tahriri, D. Vashaee, L. Tayebi, Synthesis and optical properties of cysteamine-capped ZnS quantum dots for aflatoxin quantification. J. Alloy. Compd. **690**, 749–758 (2017)
21. J. Kim, B.T. Huy, K. Sakthivel, H.J. Choi, W.H. Joo, S.K. Shin, M.J. Lee, Y.I. Lee, Highly fluorescent CdTe quantum dots with reduced cytotoxicity—a robust biomarker. Sens. Bio-Sens. Res. **3**, 46–52 (2015)
22. S.K. Vaishanav, J. Korram, P. Pradhan, K. Chandraker, R. Nagwanshi, K.K. Ghosh, M.L. Satnami, Green luminescent CdTe quantum dot based fluorescence nano-sensor for sensitive detection of arsenic (III). J. Fluoresc. **27**(3), 781–789 (2017)
23. F. Kogelheide, K. Kartaschew, M. Strack, S. Baldus, N. Metzler-Nolte, M. Havenith, P. Awakowicz, K. Stapelmann, J.W. Lackmann, FTIR spectroscopy of cysteine as a ready-to-use method for the investigation of plasma-induced chemical modifications of macromolecules. J. Phys. D Appl. Phys. **49**(8), 084004 (2016)
24. M.J. Farrell, R.J. Reaume, A.K. Pradhan, Visual detection of denatured glutathione peptides: a facile method to visibly detect heat stressed biomolecules. Sci. Rep. **7**(1), 1–11 (2017)
25. J. Kaur, V. Kumar, K.B. Tikoo, S. Bansal, A. Kaushik, S. Singhal, Glutathione modified fluorescent CdS QDs synthesized using environmentally benign pathway for detection of mercury ions in aqueous phase. J. Fluoresc. **30**(4), 773–785 (2020)
26. S. Sapra, D.D. Sarma, Evolution of the electronic structure with size in II–VI semiconductor nanocrystals. Phys. Rev. B **69**(12), 125304 (2004)
27. S. Sapra, N. Shanthi, D.D. Sarma, Realistic tight-binding model for the electronic structure of II–VI semiconductors. Phys. Rev. B **66**(20), 205202 (2002)
28. X. Peng, J. Wickham, A.P. Alivisatos, Kinetics of II-VI and III-V colloidal semiconductor nanocrystal growth: "focusing" of size distributions. J. Am. Chem. Soc. **120**(21), 5343–5344 (1998)
29. W.W. Yu, L. Qu, W. Guo, X. Peng, Experimental determination of the extinction coefficient of CdTe, CdSe, and CdS nanocrystals. Chem. Mater. **15**(14), 2854–2860 (2003)
30. A. Priyam, S. Ghosh, S.C. Bhattacharya, A. Saha, Supersaturation driven tailoring of photoluminescence efficiency and size distribution: a simplified aqueous approach for producing high-quality, biocompatible quantum dots. J. Colloid Interface Sci. **333**(1), 195–201 (2009)
31. S. Modes, P. Lianos, Luminescence probe study of the conditions affecting colloidal semiconductor growth in reverse micelles and water-in-oil microemulsions. J. Phys. Chem. **93**(15), 5854–5859 (1989)
32. R. Viswanatha, D.D. Sarma, Study of the growth of capped ZnO nanocrystals: a route to rational synthesis. Chem. Eur. J. **12**(1), 180–186 (2006)
33. T. Sugimoto, Preparation of monodispersed colloidal particles. Adv. Colloid Interface Sci. **28**, 65–108 (1987)
34. D.V. Talapin, A.L. Rogach, M. Haase, H. Weller, Evolution of an ensemble of nanoparticles in a colloidal solution: theoretical study. J. Phys. Chem. B **105**(49), 12278–12285 (2001)
35. A. Chatterjee, A. Priyam, S.C. Bhattacharya, A. Saha, Differential growth and photoluminescence of ZnS nanocrystals with variation of surfactant molecules. Colloids Surf A **297**(1–3), 258–266 (2007)
36. S. Kanagasubbulakshmi, K. Kadirvelu, Nano interface potential influences in CdTe quantum dots and biolabeling. Appl. Nanosci. **8**(3), 285–295 (2018)